Can filaments, pellets and powder be used as feedstock to produce highly drug-loaded ethylene-vinyl acetate 3D printed tablets using extrusion-based additive manufacturing?

Can filaments, pellets and powder be used as feedstock to produce highly drug-loaded ethylene-vinyl acetate 3D printed tablets using extrusion-based additive manufacturing?

Aseel Samaro[a,b], Bahaa Shaqour[c,d], Niloofar Moazami Goudarzi[e], Michael Ghijs[f], Ludwig Cardon[g], Matthieu N. Boone[e], Bart Verleije[h], Koen Beyers[h], Valérie Vanhoorne[a], Paul Cos[c], Chris Vervaet[a,*]

[a] Laboratory of Pharmaceutical Technology, Faculty of Pharmaceutical Sciences, Ghent University, Ghent, Belgium

[b] Pharmacy Department, Faculty of Pharmacy, Nursing and Health Professions, Birzeit University, Palestine

[c] Laboratory for Microbiology, Parasitology and Hygiene (LMPH), Faculty of Pharmaceutical, Biomedical and Veterinary Sciences, University of Antwerp, Belgium

[d] Mechanical and Mechatronics Engineering Department, Faculty of Engineering & Information Technology, An-Najah National University, Palestine

[e] Radiation Physics–Centre for X-ray Tomography, Department of Physics and Astronomy, Ghent University, Belgium

f Laboratory of Pharmaceutical Process Analytical Technology, Faculty of Pharmaceutical Sciences, Ghent University, Belgium

[g]Centre for Polymer and Material Technologies (CPMT), Department of Materials, Textiles and Chemical Engineering, Ghent University, Belgium

[h] Voxdale bv, Wijnegem, Belgium

Corresponding author:

Chris Vervaet
Ghent University
Laboratory of Pharmaceutical Technology
Ottergemsesteenweg 460
9000 Ghent (Belgium)
Tel.: +32 9 264 80 54
Fax: +32 9 222 82 36
E-mail: Chris.Vervaet@Ugent.be

Graphical abstract

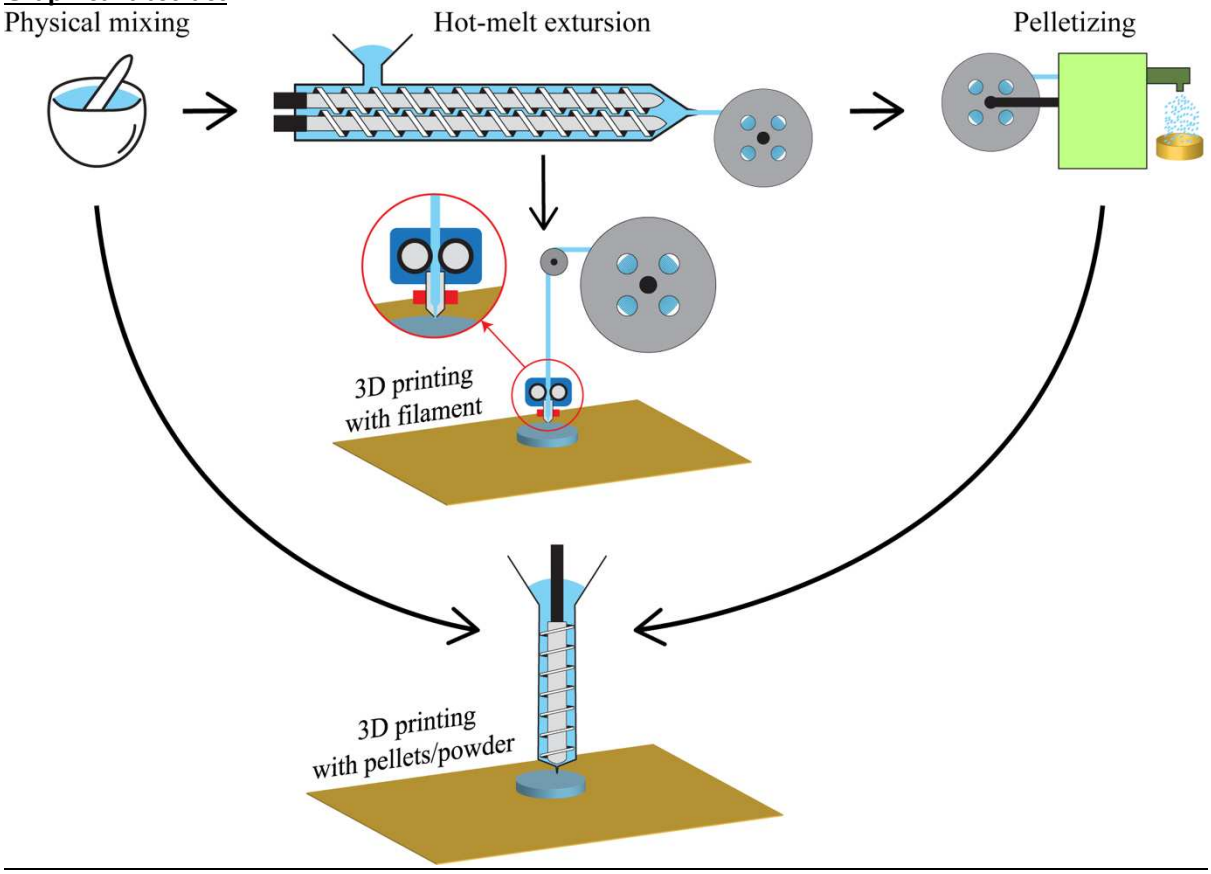

Abstract

Personalized medicine, produced through 3D printing, is a promising approach for delivering the required drug dose based on the patient's profile. The primary purpose of this study was to investigate the potential of two different extrusion-based additive manufacturing techniques – fused filament fabrication (FFF) and screw-based 3D printing, also known as direct extrusion additive manufacturing (DEAM). Different ethylene-vinyl acetate (EVA) copolymers (9%VA, 12%VA, 16%VA, 18%VA, 25%VA, 28%VA, and 40%VA) were selected and loaded with 50% (*w/w*) metoprolol tartrate (MPT). Hot-melt extrusion was performed to produce the drug-loaded filaments. These filaments were used for FFF in which the mechanical and rheological properties were rate-limiting steps. The drug-loaded filament based on the 18%VA polymer was the only printable formulation due to its appropriate mechanical and rheological properties. As for the highest VA content (40%VA), the feeding pinch rolls cause buckling of the filaments due to insufficient stiffness, while other filaments were successfully feedable towards the extrusion nozzle. However, poor flowability out of the extrusion nozzle due to the rheological limitation excluded these formulations from the initial printing trials. Filaments were also pelletized and used for pellets-DEAM. This method showed freedom in formulation selection because the screw rotation drives the material flow with less dependence on their mechanical properties. All drug-loaded pellets were successfully printed via DEAM, as sufficient pressure was built up towards the nozzle due to single screw extrusion processing method. In contrast, filaments were used as a piston to build up the pressure required for extrusion in filament-based printing, which highly depends on the filament's mechanical properties. Moreover, printing trials using a physical mixture in powder form were also investigated and showed promising results. *In vitro* drug release showed similar release patterns for MPT-loaded 3D printed tablets regardless of the printing technique. Additionally, pellets-DEAM enabled the production of tablets with the highest VA content, which failed in FFF 3D printing but showed an interesting delayed release profile.

Keywords

Ethylene-vinyl acetate
3D printing
Additive Manufacturing
Hot melt extrusion
Fused Filament Fabrication
Screw-based 3D printing
Extrusion based additive manufacturing
Direct Pellet Additive Manufacturing
Drug delivery systems

1. Introduction

In recent years, fused filament fabrication (FFF) has emerged as an interesting manufacturing technique for pharmaceutical dosage forms in the context of personalized medicine [1–5]. Conventionally, this technique starts from filament production via hot-melt extrusion (HME). Subsequently, these thermoplastic filaments are fed via rotating pinch rolls to the printer nozzle, which is heated to a specific temperature to melt and liquefy the filament in order to deposit it layer-by-layer on the building plate [6–8]. However, different studies have shown some limitations to this 3D printing technique, as it was demonstrated that filaments should have suitable mechanical and rheological properties to enable smooth processing [9,10]. Filaments that are too brittle will break between the feeding rolls, whereas filaments with low stiffness will not act as a piston to maintain a constant material flow during printing [11,12]. Suitable rheological properties are also required to enable sufficient flow through the printer nozzle [7,13–16]. As a result, the material choice for FFF is limited, and extensive research is required to modify the filament properties by adding different excipients.

Alternatively, powder or pellets can also be used as the feedstock material for direct extrusion additive manufacturing (DEAM) [17,18]. In this setup, the screw rotation mainly drives the material flow towards the printer nozzle. Hence, specific mechanical properties for filament printing are not required. This enables researchers to explore a broader range of formulations for 3D printing, allowing more flexibility for optimizing the drug release profile from 3D printed dosage forms. Several studies have already explored the possibility of producing drug delivery systems using DEAM. Goyanes et al. [19] investigated the use of screw-based 3D printing by printing of powder mixtures to prepare solid dosage forms where hydroxypropylcellulose (HPC)/indomethacin tablets were successfully prepared. Additionally, Fanous et al. [20] investigated the applicability of producing solid dosage forms using a piston-driven extrusion system, also known as syringe-based additive manufacturing. Physical mixtures containing HPC as a polymeric carrier and caffeine as a model drug were fed into a heated syringe and successfully 3D printed into rapid-release tablets. Finally, Shaqour et al. [21] investigated the effect of mixing approaches on the efficacy of implantable drug delivery systems using a screw-based 3D printer. Polycaprolactone and gentamicin sulfate were used as a polymeric carrier and model drug, respectively.

Formulations based on ethylene-vinyl acetate (EVA) polymers (Figure 1) were extensively studied for preparing sustained release dosage forms due to their hydrophobic characteristics. Moreover, as the glass transition of EVA is low, it is a suitable candidate for heat-based processing techniques such as HME and 3D printing [22]. EVA is a semicrystalline copolymer of ethylene (E) and vinyl acetate (VA),

where varying the VA content modifies the physical and mechanical properties from rigid (at low VA content) to rubbery (at high VA content). This versatility in the physicochemical properties makes EVA polymers interesting for studying in 3D printing applications. Genina et al. [23] designed EVA-based intrauterine systems through FFF. Although EVA formulations with VA content ranging from 9 to 33% loaded with indomethacin were tested, only formulations with VA content of 9, 16, and 18% were printable. The main challenge for producing solid dosage forms via FFF 3D printing using EVA as a matrix excipient was the high filament flexibility which could not act as a piston to push the melted polymer through the nozzle.

In this study, we compared the effectiveness of FFF and DEAM technologies for the processing of EVA-based formulations containing a high drug load. We studied the effect of the EVA grade on the mechanical and rheological characteristics of drug-loaded filaments and on the release pattern of tablets manufactured via the different 3D printing technologies.

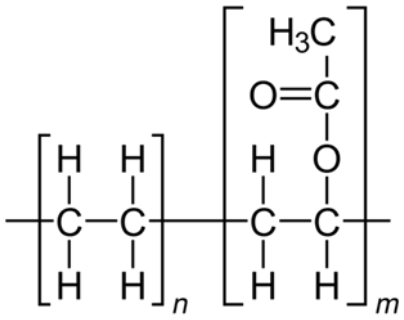

Figure 1: General structure of ethylene-vinyl acetate (EVA)

2. Experimental section

2.1 Materials

Metoprolol tartrate (MPT) (Utag, Netherlands) was used as a model drug in combination with ethylene-vinyl acetate (EVA) polymer. MPT is highly water-soluble (50 mg/mL at 25 °C) with a degradation temperature of 160 °C. A range of EVA grades with different VA content (Ateva 1070, 1241, 1615, 1850A, 2604A, 2825A, and 4030AC), donated by Celanese (Germany), was included to study their 3D printing performance. Throughout this paper, the previously mentioned grades will be noted by their VA content (Table 1).

Table 1: General properties for the EVA grades evaluated in the study

	1070 (9%VA)	1241 (12%VA)	1615 (16%VA)	1850A (18%VA)	2604A (25%VA)	2825A (28%VA)	4030AC (40%VA)
VA content (%)	9	12	16	18	25	28	40
MFI* (g/min)	0.28	1.0	1.5	15.0	0.45	4.3	5.5
Crystallinity** (%)	19.7	15.5	13.6	12.9	8.0	5.3	4.9

* MFI values (g/min) measured at a barrel temperature of 190°C and using a load cell of 2.160 kg (reported by Celanese™)
**Crystallinity was calculated based on the enthalpy of fusion of perfect polyethylene crystal (277.1 J/g)

2.2 Hot melt extrusion: production of filaments and pellets

Physical mixtures (500 g) of MPT/EVA (50/50; *w/w*%) were prepared using a tumbling mixer (Inversina, Bioengineering, Switzerland) for 15 min at 25 rotations per minute (rpm). Subsequently, the physical mixture was fed into a Prism Eurolab 16 co-rotating twin-screw extruder (Thermo Fisher Scientific, Germany) using a DD flex- wall® 18 gravimetric feeder (Brabender Technology, Germany) and a feed rate of 0.25 kg/h. The extruder was equipped with a barrel length of 25 L/D (where L is the machine axial screw length, and D is the inner bore diameter). An in-house custom-made die with a diameter of 1.75 mm was used to collect filaments with a suitable diameter. A standard screw configuration was used for all experiments with three kneading zones (L = D/4) and four conveying zones. The barrel temperature was adjusted based on the EVA grade, as shown in Table 2. The screw speed was set to 100 rpm for all experiments. The extruded filament was collected on a rotating spool at room temperature. If required, the speed of the spool was adjusted to stretch the filaments to the desired diameter. Subsequently, part of these filaments was pelletized using a pelletizer (type 12-72-000 Brabender Technology, Germany) to form pellets with 1.75 mm diameter and 3 mm length.

2.3 Mechanical properties of the filaments

The mechanical properties of the filaments were evaluated through tensile, three-point bend, and buckling tests to study their feeding behavior into a filament-based 3D printer. All mechanical tests were performed using a TA.HDplusC Texture Analyzer (Stable Micro Systems, United Kingdom) equipped with a 30 kg load cell. Data from the texture analyzer were collected via v.8.0 Exponent Connect software (Stable Micro Systems, United Kingdom). All data was analyzed using v.2020B Matlab (The Mathworks, United States of America).

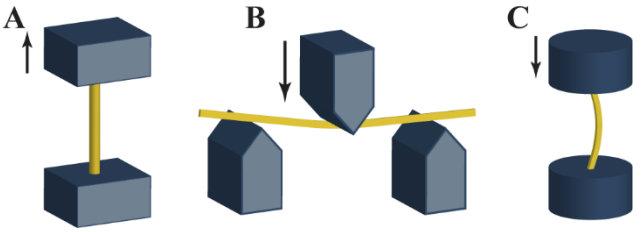

Figure 2: The different configurations used for testing the mechanical properties of the drug-loaded filaments via tensile (A), three-point bending (B), and buckling (C) tests.

2.3.1 Tensile test

A tensile test was performed to study the stiffness of MPT-loaded filaments formulated with different EVA grades. During the test, filaments were stretched to a maximum distance of 140 mm using a TA-243 self-tightening roller grip system (Stable Micro Systems, United Kingdom) (Figure 2A). The test speed and the initial distance of separation were set at 3 mm/s and 20 mm, respectively. A stress-strain curve was plotted for all filaments, as described by Samaro et al. [7]. The tensile elastic modulus (EM) was calculated using a linear interpolation within 1% and 5% strain from the generated stress-strain curve (*n*=3).

2.3.2 Three-point bend test

A three-point bend test was performed to study the flexural modulus of the drug-loaded filaments and relate these to the filament feedability into the 3D printer. This test was conducted as reported by Prasad et al. [14]. A TA-95N testing rig (Stable Micro Systems, United Kingdom) was used with a gap of 8 mm (Figure 2B). Filaments were cut into 20 mm long samples. The test speed was set to 0.02 mm/s with a maximum displacement of 20 mm. The stress and strain of each sample was calculated from the force-displacement data based on Equation 1 and Equation 2, respectively. The flexural elastic modulus was calculated using a linear interpolation within 1.5% and 5% strain from the generated stress-strain curve (*n*=5).

$$\sigma_f = \frac{FL}{\pi R^3} \quad \text{Equation 1}$$

σ_f is the flexural stress (MPa)
F is the applied force (N)
L is the gap (mm)
R is the radius of the specimen (mm)

$$\varepsilon_f = \frac{600sh}{L^2}$$ Equation 2

ε_f is the flexural strain (%)
s is the deflection (mm)
h is the thickness of the test specimen (mm)
L is the gap (mm)

2.3.3 Buckling test

A modified buckling test based on a study by Nasereddin et al. [24] was performed to compare the filaments in terms of their maximum allowable axial compression load (buckling behavior). The test was performed using an in-house developed gripper. Two aluminum cylinders with a concentric hole of 1.8 mm diameter and 10 mm depth were designed. Each cylinder was fixed in the texture analyzer with a distance of 40 mm between them (Figure 2C). The test was conducted with a speed of 2 mm/s and a maximum displacement of 15 mm. Before testing, filaments were cut into 60 mm long samples to achieve consistent maximum buckling load results. Samples that did not show pure buckling (Supplementary video 1) behavior were discarded and five repetitions per formulation were used for the analysis. The stress-strain curve was recorded, with the average maximum stress for each formulation, reported as the buckling stress.

2.4 Rheological properties of filaments

To investigate the rheological properties of different MPT/EVA filaments, frequency sweeps were performed at the printing temperature (130 °C) using a stress-controlled HAAKE Mars III rheometer (Thermo Scientific, Germany). Filaments were loaded onto a parallel plate geometry with a 20 mm diameter. After melting of the filament, the gap size was reduced to 1 mm, excess material was trimmed and the sample was equilibrated for 15 min. Prior to the frequency sweeps, the linear viscoelastic region was determined by performing an amplitude sweep experiment over a strain range (0.1–10%). Subsequently, frequency sweeps were performed at a strain deformation of 1%.

2.5 3D printing of tablets

For both printing techniques flat-faced cylindrical tablets were manufactured with a diameter and height of 10.00 and 3.00 mm, respectively. The geometry of the printed object was designed as an STL file format using Sketch up (Trimble, United States of America).

2.5.1 3D printing using FFF technology

The filament feeding performance was tested using a Prusa i3 MK3S printer (Prusa Research, Czech Republic). Filaments that were successfully forwarded towards the printer nozzle were defined as "feedable filaments." In contrast, filaments that failed to feed due to buckling were defined as "non-feedable filaments." Subsequently, feedable filaments were tested for their printability, and promising filaments were used to print tablets. A printing temperature of 130 °C was used, in combination with

a layer height of 0.25 mm, 2 external shells, 100% rectilinear infill, 10 mm/s printing speed for all layers and a nozzle diameter of 0.4 mm. No raft was used and the building platform temperature was set to 20 °C.

2.5.2 3D printing using DEAM technology

The drug-loaded filaments were pelletized into pellets with 1.75 mm diameter and 3 mm length for pellets-DEAM. On the other hand, a physical mixture of MPT/18%VA (50:50% *w/w*) was prepared using a mortar and pestle to test the possibility of powder-DEAM.

The extrusion head of a conventional da Vinci 1.0 FFF 3D printer (XYZPrinting, the Netherlands) was replaced with a mini screw extrusion head (MAHORXYZ, Spain). The screw has a diameter of 8.00 mm, a pitch of 8.50 mm, a channel width of 7.00 mm, and a helix angle of 24°. The variable channel depth was 2.50 mm and 1.00 mm for the feeding section and the metering section, respectively. The hopper section was redesigned (Figure 3) to allow feeding pellets (Figure 3A) and powder (Figure 3B). The hopper wall used for powder extrusion was steeper with an angle of 13° compared with 32° for the hopper designed for pellets. Additionally, an agitator arm was attached to the screw in the design used for powder extrusion to scrape the walls of the hopper and the improve the flowability of the material towards the extruder. Moreover, the redesign considered the ease of disassembling the extruder parts to allow accessibility for cleaning with minimum time when changing between formulations. The printer controller was exchanged with an open source (Duet 2 WIFI controller, United Kingdom) to set the firmware parameters more easily. Moreover, Slic3r (v.1.3) software was used to set the printing parameters.

A layer height of 0.25 mm, 2 external shells, 100% rectilinear infill, and 10 mm/s printing speed were selected. The printing temperature used in this study was 130°C and the nozzle diameter was 0.4 mm. The extrusion multiplier (EM) parameter is a tool that controls the extruded amount (volume) of material in the unit distance traveled by the printing head [25]. The EM was used for fine-tuning the material flow in order to improve the dimensions of the printed part [26]. In this study, the extrusion multiplier was used to cope with the melt viscosity variations for the different EVA formulations and was set in a range between 0.026 up to 0.08, depending on the formulation.

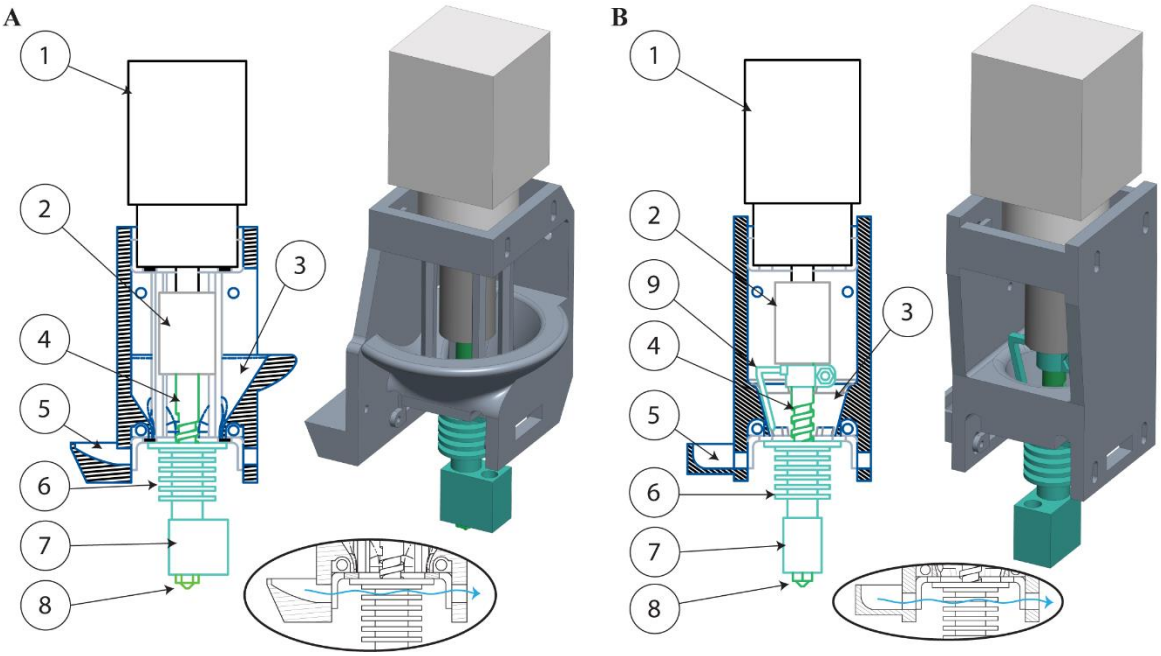

Figure 3: Illustration of the modified extrusion head used for pellet (A) and powder (B) printing. The zoomed section shows the cooling streamflow to avoid heat escape from the barrel section to the hopper. Numbered component key: (1) motor and gear, (2) coupler, (3) hopper, (4) screw, (5) cooling stream inlet, (6) barrel with heat sink, (7) heater, (8) nozzle and (9) agitator arm.

2.6 Tablet characterization

2.6.1 Content uniformity

The content uniformity of MPT in the 3D printed tablets was analyzed by placing an MPT/EVA tablet into a 100 ml volumetric flask containing purified water. The flask was shaken for 48 hours to allow the MPT fraction to dissolve. The resulting MPT solution was filtered, diluted and analyzed at a wavelength of 223 nm using a UV-1650PC spectrophotometer (Shimadzu Benelux, Belgium). The test was done in triplicate.

2.6.2 Drug homogeneity by near infrared-chemical imaging

The drug homogeneity in the 3D-printed tablets was assessed using near-infrared-chemical imaging (NIR-CI) or hyperspectral imaging. Hyperspectral images contain spectral information at a high resolution within every pixel of the image. Hyperspectral measurements were conducted with a line-scanning push-broom-configured camera (VLNIR-CL-100-N173, Specim, Finland). The samples were illuminated by a halogen lamp with a radiating light at an angle of 45°. An ImSpector N17E imaging spectrograph captures the sample's reflection in the wavelength region of 900 – 1700 nm through a temperature-stabilized InGaAs camera, with a spectral resolution of 256 wavelengths. By using the OLES Macrolens, the width of the scanned line was 1 cm. As the line scan is composed of 320 pixels,

the resulting resolution is 31.25 µm. The camera was fixed, and the tablets were moved underneath it to create the 2D hyperspectral image of the tablet based on 470 consecutive line scans. Every pixel of this image contains the spectral information recorded as per the resolution and range mentioned above.

The recorded images were preprocessed for different aspects: dead pixel removal, spectral smoothing (Savitzky-Golay, 11 point window, first-order polynomial), background removal and standard-normal-variate normalization (SNV) [27,28]. The background omittance from the image was based on principal component analysis (PCA) of the smoothed spectra. This was done before SNV normalization, as the SNV step aims to correct the sample's morphology.

After the preprocessing, the chemical composition at each point/pixel imaged on the tablet was analyzed using PCA, which was executed on the normalized spectra. The variance in spectra across the tablet was decomposed orthogonally. The corresponding loadings were assessed for their correspondence to the pure spectra of the original components. The spectral variance across the tablet is thus related to the compounds' spectra that make up the tablet [29].

2.6.3 *In vitro* dissolution

The drug release characteristics of the 3D printed tablets were evaluated using a PTWS 120D dissolution bath (Pharma test, Germany). The temperature and paddle speed were set to 37 ± 0.5 °C and 100 rpm, respectively. Purified water (900 mL) was used as dissolution medium. A sample of 5.0 mL was taken at ten time points (0.5, 1, 2, 4, 6, 8, 12, 16, 20 and 24 h). The absorbance of these samples was measured at a wavelength of 223 nm using a UV-1650PC spectrophotometer (Shimadzu Benelux, Belgium).

To compare the drug release rate from tablets 3D printed via FFF and powder/pellets-DEAM technologies, the Korsmeyer-Peppas model (Equation 3) was used. After curve fitting, the release rate (k) was calculated based on data points up to 65% of the total released drug. Subsequently, statistical analyses using two-way ANOVA and Tukey test was used to determine the potential statistical differences between the data. *P*-values above 0.05 was considered statistically different. Custom v.2020B Matlab (The Mathworks, United States of America) code was used for the curve fitting and statistical analyses.

$$\frac{C_t}{C_\infty} = kt^n \quad \text{Equation 3}$$

C_t/C_∞ is the fraction of drug released
k is the rate constant
n is the release exponent which was 0.5 for tablet geometry [21]

2.6.4 Micro computed tomography analysis (μCT)

X-ray tomography was used to evaluate the total porosity, maximum opening, and equivalent diameter of the pores in 3D printed tablets formulated with EVA grades 9%VA and 40%VA before and after 24 hrs dissolution.

Imaging was performed using the High Energy CT system optimized for research at Ghent University Center for X-ray Tomography (UGCT) [30] in which the source was operated at a voltage of 90 kV and a target power of 10 W. 2400 projections were taken with an exposure time of 1 second per image for a full 360° rotation. All scans were reconstructed using Octopus Reconstruction into a 3D volume (stored as a stack of 2D images) at a voxel size of 7^3 μm^3. At the given tube settings, the spatial resolution is almost not affected by the focal spot size. The in house developed Octopus Analysis software package was used for the 3D analysis of the reconstructed data to characterize the tablet's porosity and pore distribution [31].

The total porosity was calculated as the percentage of a tablet's pore volume to its total volume. The equivalent diameter is the diameter of a sphere with the same volume as the pore, while the maximum opening is the diameter of the largest inscribed sphere in the object. The porosity, equivalent diameter and maximum opening were all calculated in 3D based on the entire 3D volume. To visualize the tablet in virtual 3D volume, the stack of 2D images was rendered using VGSTUDIO MAX (Volume Graphics, Heidelberg, Germany).

2.6.5 Differential scanning Calorimetry

Differential scanning calorimetry (DSC) (Q2000, TA instruments, United Kingdom) was used to determine the drug crystallinity in the 3D printed tablet. A sample of 5-10 mg was filled into non-hermetically sealed Tzero pans (TA instruments, Belgium). A single heating run from 0 to 150 °C was performed at a heating rate of 10 °C/min. The DSC apparatus was equipped with a refrigerated cooling system and dry nitrogen at a flow rate of 50 mL/min. The percentage of drug crystallinity was calculated by means of Equation 4 using the melt enthalpy obtained in DSC experiments.

$$Xc = \frac{\Delta H1}{f \times \Delta H2} \times 100 \quad \text{Equation 4}$$

Xc is the crystallinity percentage
$\Delta H1$ is the melt enthalpy of MPT into the 3D printed tablet
$\Delta H2$ is the melt enthalpy of pure MPT
f is the fraction of drug in formulation (50% w/w)

The crystallinity of pure polymer was also estimated (Eq. 5) by DSC using the same method, based on the melting enthalpy of a perfect polyethylene (PE) crystal (277.1 J/g).

$$Xc = \frac{\Delta H1}{\Delta H2} \times 100$$ Equation 5

Xc is the crystallinity percentage
$\Delta H1$ is the melt enthalpy of EVA
$\Delta H2$ is the melt enthalpy of perfect PE

Modulated DSC measurements were carried out to determine the glass transition of pure polymers. The temperature's amplitude was 0.3 °C over 50 seconds, and the underlying heating rate was 2 °C/min. The samples were evaluated from -100 to 150 °C.

3. Results and discussion

3.1 Filament production via HME

MPT/EVA filaments were extruded successfully, independent of the EVA grade. The filament's visual appearance was excellent with a smooth surface morphology despite the high drug load (50% *w/w*). The filament diameter could be adjusted by the rotating spool to the diameter required for filament-based 3D printing using the Prusa printer (1.75 ± 0.5 mm). In general, a higher temperature was needed to extrude EVA grades with lower VA content, as shown in Table 2. This was due to the larger crystalline fraction in EVA grades with low VA content, which was also evident from the DSC thermograms shown in Figure 4.

EVA grades with a high VA content were more flexible, which was also noted when handling the filaments after HME. The glass transition temperatures of the EVA grades were about -30 °C, as shown in Figure 4, making EVA flexible at room temperature. However, as reported by Almeida et al. and displayed in the DSC thermograms (insert in Figure 4), the heat capacity involved in the glass transition step increased at higher VA content which corresponds to the difference in the polymer flexibility [22]. The amorphous region of the EVA polymer consists of two areas: a rigid boundary amorphous region and a mobile amorphous region. When heat is applied, the mobile amorphous phase, with its free movements, corresponds to the heat capacity change during the glass transition step (40%VA). In contrast, the rigid amorphous phase, which is integrated between the crystalline chains, will not contribute to the glass transition step (9%VA). This means that EVA with a higher VA content has a more mobile amorphous phase and higher flexibility, indicated by the high heat capacity step [22,32].

Table 2: Overview of the extrusion temperature (°C) and torque values (%) during HME for different EVA grades loaded with 50% (w/w) MPT.

EVA grade	9%VA	12%VA	16%VA	18%VA	25%VA	28%VA	40%VA
Extrusion temperature (°C)	110	100	90	80	80	70	70
Torque* (%)	40	35	32	30	39	38	35

*The maximum torque (100%) corresponds to 24 N.m equally divided on each shaft.

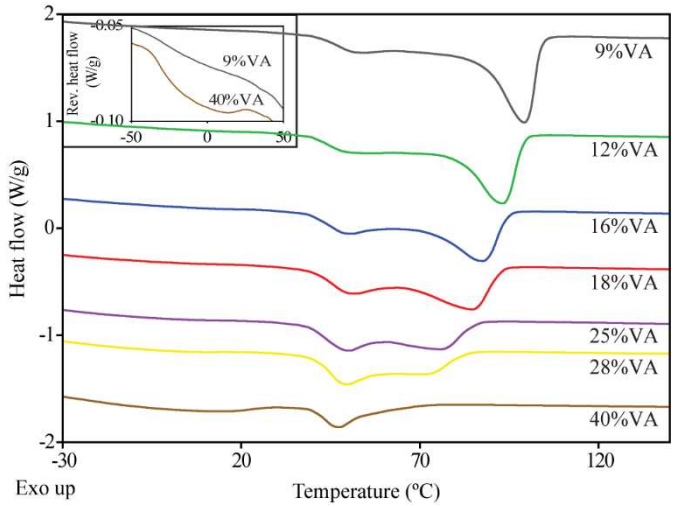

Figure 4: DSC thermograms of the different pure EVA grades, the insert shows the MDSC analysis focusing on the glass transition steps of EVA grades 9%VA and 40%VA.

3.2 Tablet printing via fused filament fabrication (FFF)

FFF 3D printing involves three main steps: feeding the filaments through the rotating rolls, extruding the liquefied filament through a well-defined nozzle, and solidifying the 3D object on the building plate. Various studies concluded that filaments used as feedstock material in FFF should exhibit specific characteristics to allow the feeding and printing steps [6,7,13,15,33,34]. The filaments should have suitable mechanical properties to allow feeding towards the printing nozzle. Brittle filaments will not withstand the feeding pinch rolls, and therefore they will break between them. However, filaments that are too flexible will not be stiff enough to be pushed towards the printer nozzle, and they will buckle and bend. In addition, filaments should exhibit suitable rheological properties to flow through the nozzle. The materials should also have acceptable thermal properties, as FFF 3D printing involves heating and melting of the filament and solidifying of the melt on the build platform.

3.2.1 Feedability

Throughout the feeding process, filaments pass through the feeding pinch rolls that should grip the filament from both sides with minimal contact. When the contact area increases between the rolls and a flexible filament, the filament tends to wind onto the rotating roll. Preliminary feeding trials with pure EVA filaments using the Prusa Printer showed that EVA filaments with high VA content (25%VA, 28%VA, and 40%VA) were bent by the feeding pinch rolls as the higher VA content of these grades resulted in high flexibility of the filaments**Error! Reference source not found.**). However, the addition of MPT increased the stiffness of the EVA filament as all drug-loaded filaments were successfully fed towards the nozzle, except for the highest VA content (40%VA) (Table 3). This was reflected in the rank of order of the MPT-loaded EVA filaments based on the elastic modulus (Figure

5A) and flexural modulus (Figure 5B), which confirmed the observations made during handling the filaments: 9%VA, 12%VA, 16%VA, 18%VA, 25%VA, 28%VA, and 40%VA. The lower elastic modulus of the MPT-40%VA filament resulted in buckling of the filament by the feeding pinch rolls due to its lower stiffness. This prevented it from acting as a piston to generate the pressure needed for extrusion and to push the melted material out of the nozzle. The axial compression of the filament between the pinch rolls and the nozzle also exposed the material to bending forces. Hence due to its low flexural modulus, the filaments containing 40%VA could not withstand the compression forces and was bent between the pinch rolls and the nozzle. On the other hand, the buckling stress represents the maximum axial compression load the filament can endure before starting a severe axial deformation. Once the buckling stress is reached, the filament can easily wind onto one of the rotating rolls. Significant low buckling stress was observed for the MPT/40%VA filament which showed buckling during the feeding step (Figure 5C).

Figure 6 represents the effect of increasing the VA content on reducing the filament's maximum buckling stress, the elastic and flexural modulus making it more prone to bending. Apart from MPT/40%VA feeding failure, other higher drug-loaded VA content (25%VA, 28%VA) filaments were occasionally bent during the feeding step, affecting the reproducibility of the process.

Table 3: Overview of the feedability and printability during filament-based 3D printing and the extrusion multiplier used during screw-based 3D printing for the different EVA grades loaded with 50% (w/w) MPT.

	EVA grade	9%VA	12%VA	16%VA	18%VA	25%VA	28%VA	40%VA
Filament-based	Feedability	✔	✔	✔	✔	✔	✔	✗
	Printability	✗	✔	✔	✔	✗	✔	✗
Screw based	Extrusion Multiplier	0.026	0.023	0.023	0.024	0.055	0.08	0.08

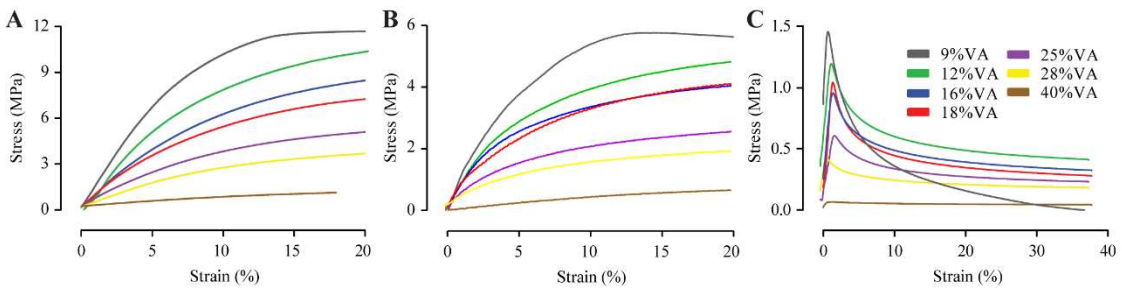

Figure 5: Stress-strain curves for dug loaded EVA filaments obtained from the tensile test (A), 3-point bend test (B) and buckling test (C).

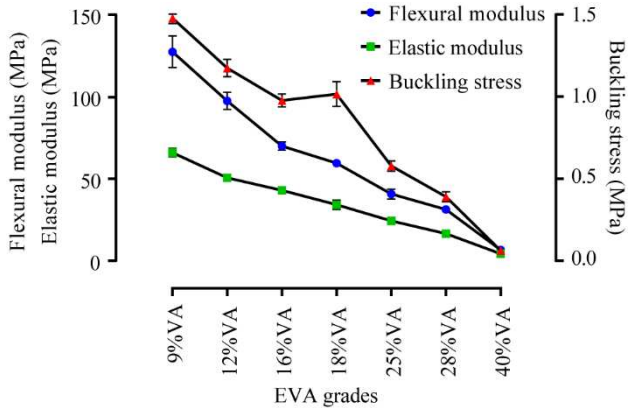

Figure 6: Elastic modulus, flexural modulus and buckling stress (MPa) for dug loaded EVA filaments obtained from tensile tests, 3-point bend test and buckling test, respectively.

3.2.2 Printability

Printability can be defined as the melt's ability to continuously flow out of the extrusion nozzle mainly depending on the melt viscosity [16,34]. Therefore, the rheological properties of the formulations were tested to understand the printing behavior during FFF. The printing temperature used during this study was 130°C considering that the melting and the degradation temperature of MPT were 120°C and 160°C, respectively.

The drug-loaded EVA filaments showed different printing behaviors, which were attributed to their melt viscosity. Drug-loaded filaments with 9%VA or 25%VA failed at printing due to insufficient flow, which was linked to the high initial viscosity and viscosity variation (characterized by the max/min ratio) during the frequency sweeps (Figure 7A and B). In contrast, drug-loaded 12%VA and 16%VA filaments which had a moderate initial viscosity and low max/min ratio could be printed into rough tablets due to the adequate mechanical properties of the EVA grade which allowed the generation of the pressure required for extrusion. The MPT/40%VA filament also showed a moderate initial viscosity combined with a low max/min ratio. However, these filaments could not act as a piston to push the melt due to their low stiffness.

Drug-loaded filaments with 18%VA, which showed the lowest initial viscosity and max/min ratio, exhibited optimal flow behavior, resulting in high-quality 3D printed tablets. Although filaments based on 28%VA also exhibited a low initial viscosity and max/min ratio, which enabled the printing of these filaments into tablets, the quality of the printed tablet was moderate due to the lower melting temperature of the 28%VA grade, which caused deformation during the deposition of hot strands on top of each other.

As the material flow in the 3D printing process is a non-continuous extrusion process, the flow is interrupted during the non-print movement to prevent material dripping. Hence, the shear rate fluctuates, causing changes in the viscosity of the melt. If the material shows high variation in the complex viscosity (indicated by a high max/min ratio), then the flow from the nozzle could fail as

observed for the 12%VA and 16VA% MPT-loaded filaments. This was due to a significant variation in the required extrusion pressure, which was not consistently achievable with the fast change from printing and non-printing modes during tablet printing. On the other hand, smooth printing was observed from formulations that showed low viscosity variation and thus a lower Max/Min ratio, such as MPT/18%VA.

This was in agreement with the study by Serdeczny et al. in which they showed that the required extrusion pressure varies due to the non-Newtonian behavior of the polymers during 3D printing [35].

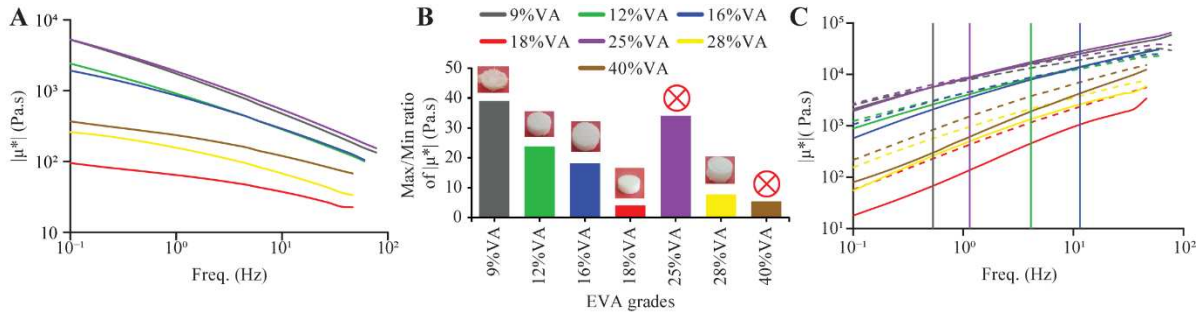

Figure 7: Complex viscosity versus frequency (A), Max/Min ratio of complex viscosity showing the 3D printed tablet using filament-based printing (B) and Loss and storage modulus versus frequency (solid line for G' and dashed line for G'') (C) for different EVA grades loaded with 50% (w/w) MPT.

3.3 Tablet printing via pellets/powder direct extrusion additive manufacturing (DEAM)

During DEAM trials, the formulations' mechanical properties were not a limiting factor for their printability as the screw rotation drives the material flow. However, a key player in this process is the melt viscosity of the formulation, which determines the extrusion temperature and the torque required for rotating the screw [18]. The single screw extruder used for 3D printing in this study (Figure 3) is divided into three sections: (1) feeding, (2) compression, and (3) metering sections [36]. The raw materials in the form of pellets or powder were fed into the feeding section, where the screw conveys them into the compression zone. An increase in the temperature due to heat transfer from the external heating element located near the nozzle softens the material. As the extruder's scale is smaller than conventional extruders, the heat transfer that occurs through the barrel is enough to heat the compression section. On the other hand, a cooling fan was placed just after the hopper to ensure that no heat escapes upward beyond the compression zone (zoomed section in Figure 3). Subsequently, the material reaches the metering section in which the cross-section of the extruder is dramatically decreased. Finally, the material exits through a nozzle and deposits on the printing platform.

As shown in Figure 7A and B, the rheological properties for the drug-loaded filaments vary based on the VA content. Moreover, the melting temperature for the different EVA grades also differs, as shown in Figure 4. However, to assure the same heat treatment for the loaded drug, 130°C was selected as printing temperature for all the formulations.

The feeding behavior was similar for most formulations with smooth feeding driven by the gravitational force. However, drug-loaded pellets with 28%VA and 40%VA grades showed softening in the feeder section due to their low melting temperature and crystallinity, as illustrated in Figure 4. On the other hand, feeding the physical mixture of 18%VA grade loaded with 50% (*w/w*) MPT (powder-DEAM) was challenging due to poor material flowability. The problem was partially solved after redesigning the hopper to achieve a smooth material flow by adding an agitator arm to avoid wall sticking and to maintain a consistent powder flow toward the rotating screw. Moreover, it is worth noting that the handling of the formulation in the powder form was not user-friendly due to the intensive cleaning process when changing between formulations. Thus, further enhancement to the configuration design should be conducted in future studies to allow a more user-friendly operation.

The extrudability of the formulation was controlled using the extrusion multiplier (EM) in the Slic3r, which is used as a fine-tuning tool to control the material flow during 3D printing [37]. The material flow was easily adjusted to obtain a smooth and continuous melt flow. Moreover, all drug-loaded pellets were successfully printed due to sufficient pressure generated by the extruder screw. The extrusion multiplier values used are shown in Table 2, indicating two ranges in function of the formulations: a low EM between 0.023 and 0.026 for 9%VA, 12%VA, 16%VA and 18%VA drug-loaded pellets, while an EM range between 0.055 and 0.08 was selected for drug-loaded 25%VA, 28%VA and 40%VA pellets. Additionally, 18%VA was 3D printed using two forms of feedstock material (powder and pellets) in order to compare with the FFF, keeping in mind that MPT/18%VA was the only good quality tablet obtained via filament printing. The EM chosen for printing the formulation in the pellet form and the powder form was 0.024 and 0.055, respectively. The smaller particle size of the powder used a feedstock material required a higher EM value since a higher screw speed was needed to compress the powder and build up the necessary extrusion pressure. This was also shown in a study conducted by Saviano et al. [38].

The printability of tablets varied based on the VA content. 3D printed tablets from 9%VA and 25%VA grade showed poor adhesion of the first layer and poor bonding between layers due to the swift change from a predominantly viscous behavior to elastic behavior, as shown in Figure 7C. Inter layer fusion is superior with a predominantly viscous behavior of the material (G''>G'), allowing the printed

strands to fuse with the previously printed layers [39][40]. All other formulations showed adequate layer adhesion due to the predominantly viscous behavior after extrusion, as shown in Figure 7C. However, tablets produced using grades 28%VA and 40%VA were slightly deformed which can be attributed to the lower melting temperatures compared to other EVA grades (Figure 4). During extrusion, the melted strands could increase the temperature of the previously deposited layer which can cause partial melting of the materials. This could be avoided by changing the processing parameters such as printing speed or temperature. Nevertheless, we aimed to print at the same printing temperature to have the equivalent MPT heat treatment.

3.4 Tablet Characterization

3.4.1 Content uniformity

Tablets produced by either FFF or pellets/powder-DEAM technologies showed content uniformity between 95% and 100% of the average content and was within the acceptable pharmacopeial ranges (Table 4**Error! Reference source not found.**). Moreover, NIR-CI also showed that MPT was homogenously distributed within the cross-sectional area of the EVA matrix regardless of the printing technique (Figure 8A to D).

Table 4: The content uniformity (%) of MPT in the 3D printed tablets using filament, pellets, and powder as feedstock material. Data expressed as the percentage of the amount of the MPT analyzed over the theoretical value.

	1070 (9%VA)	1241 (12%VA)	1615 (16%VA)	1850A (18%VA)	2604A (25%VA)	2825A (28%VA)	4030AC (40%VA)
Filament-based tablet	-	-	-	98.9 ± 1.4	-	-	-
Pellet-based tablet	97.1 ± 1.3	96.7 ± 0.9	97.2 ± 2.1	98.3 ± 1.5	95.7 ± 0.6	99.0 ± 1.4	98.1 ± 1.5
Powder-based tablet	-	-	-	96.1 ± 1.9	-	-	-

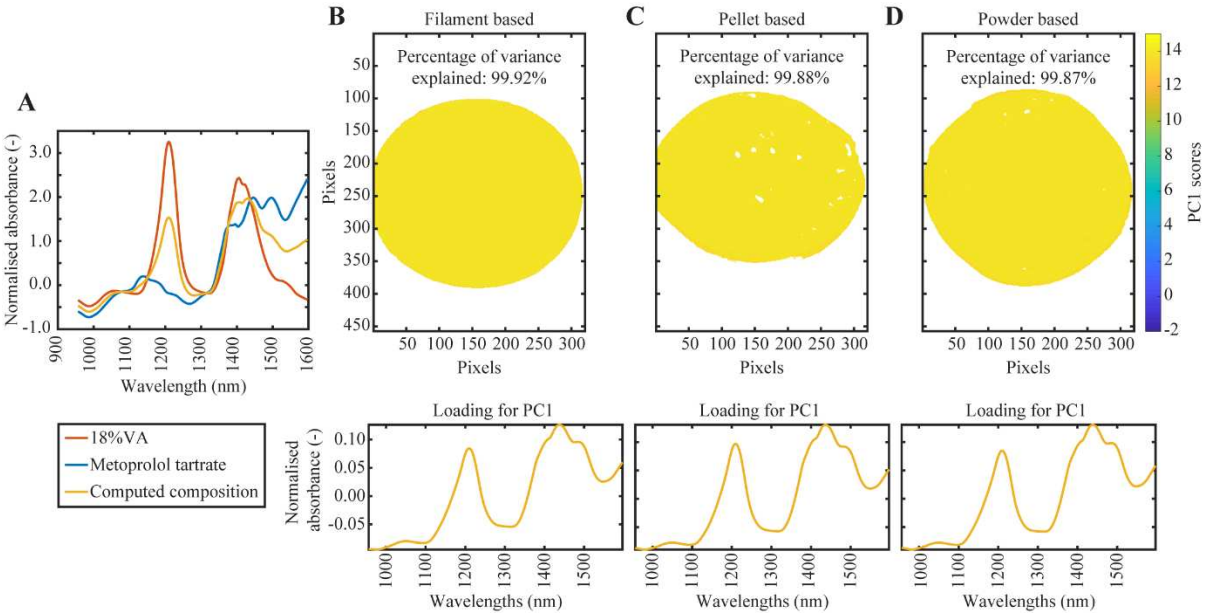

Figure 8: Pure component spectra as measured with NIR-CI and preprocessed (smoothed and normalized) along with computed normalized composition spectrum according to the Lambert-Beer law (A) and PCA results, PC1 scores per pixel in hyperspectral image (only tablet, background removed) for tablets of different printing techniques (B-D) showing the loadings of the first principal component as a function of wavelength.

Through PCA, the spectral variation across each tablet was decomposed. The first principal component (PC1) captures nearly all spectral information in the tablet (see percentage of variance explained per tablet shown in Figure 8B to D). Moreover, the scores for PC1 only varied slightly across the tablet. These observations confirmed the spectral uniformity across the tablet. The resulting loadings of PC1 also showed a clear resemblance to the computed normalized spectra of the composition, which are depicted in the lower section of Figure 8B to D. Based on this, it was concluded that the pure components were well-mixed and uniformly distributed in the tablets printed via the different techniques, which indicates that HME is not a required step for ensuring homogeneity for the final 3D printed dosage form.

3.4.2 *In vitro* drug release

The *in vitro* release characteristics of pellets were evaluated to study the release pattern based on the different EVA grades without an influence from the second heating step during printing or from the printing parameters such as the extrusion multiplier (Figure 9A).

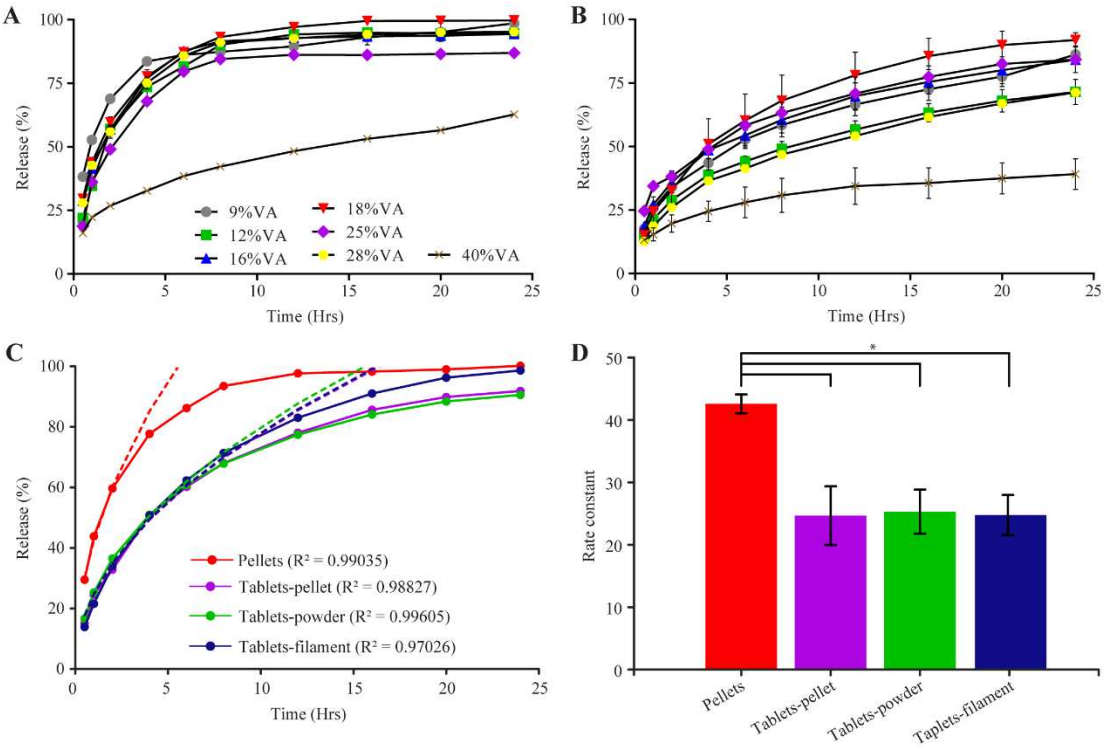

*Figure 9: In vitro release for MPT loaded pellets (A), the release from 3D printed tablets from pellets (B) and the release for 18%VA obtained from pellets, 3D printed tablets from pellets, powder and filament, dashed line shows the fitting curve based on Equation 3. (C) the rate constant calculated after curve fitting for the release from 3D tablets using different printing approaches (D). Note: Data in part D are expressed by mean ± SD with n=3 and the * indicates statistical difference at $p<0.05$.*

All tablets and pellets were still intact, keeping the same geometry after 24 hrs *in-vitro* dissolution. The drug release mechanism can be described by the diffusion of water into the matrix via the pores. This dissolves the MPT particles and allows the drug to diffuse from the matrix. This process changes the porosity and tortuosity of the matrix during dissolution. Although it was reported in the literature that a high VA content grade showed less crystallinity and less rigidity and was more permeable during dissolution [22], drug release from 40%VA pellets and tablets was significantly slower compared to the other grades (Figure 9A and B). This could be due to a more extensive structural arrangement of the 40%VA matrix during dissolution compared to other EVA grades, which is attributed to higher flexibility of this polymer. During dissolution, a collapse in the structural arrangement resulted in pore disruption. This hypothesis was also supported via µCT analysis of the EVA-based matrix tablets before and after dissolution. Figure 10 shows the pore distribution before and after dissolution based on the maximum pore opening. A significant increase in pore size of the tablet formulated with 9%VA was observed, in contrast to the minimal changes in 40%VA tablets. The total porosity after dissolution also increased by 50% and 2.7% for 9%VA and 40%VA 3D printed tablets, respectively. This indicated that the structural arrangement of 40%VA disrupted more pores created during dissolution compared to 9%VA tablets. Similar findings on the structural arrangement of EVA grades during dissolution were reported by Almeida et al. on extrudates produced by HME [22].

Figure 9C displays the release profile from drug-loaded 18%VA tablets printed using different feedstock materials. There was no significant difference between the 3D tablet printed from pellet or powder at the same temperature and printing speed (Figure 9D). This is an interesting finding, offering the flexibility to choose the printing technique based on the properties of the material. Moreover, MPT remains mainly crystalline after filament, pellets, and powder printing with 99.1, 99.4, and 99.9% crystallinity, respectively.

Genina et al. excluded several EVA-based formulations from the printing trials showing low flexural modulus, extremely high or low viscosity due to a limitation in feeding and printing using a filament-based 3D printer [23]. In contrast, in our study, all drug-loaded pellets were successfully printed regardless of the mechanical and rheological constraints faced during filament printing. Moreover, tablets based on 40%VA grades showed promising sustained release profiles but were excluded from FFF trials due to limitations in the mechanical properties. Therefore, pellets-DEAM technology was an alternative method that allows a higher flexibility in formulation choice.

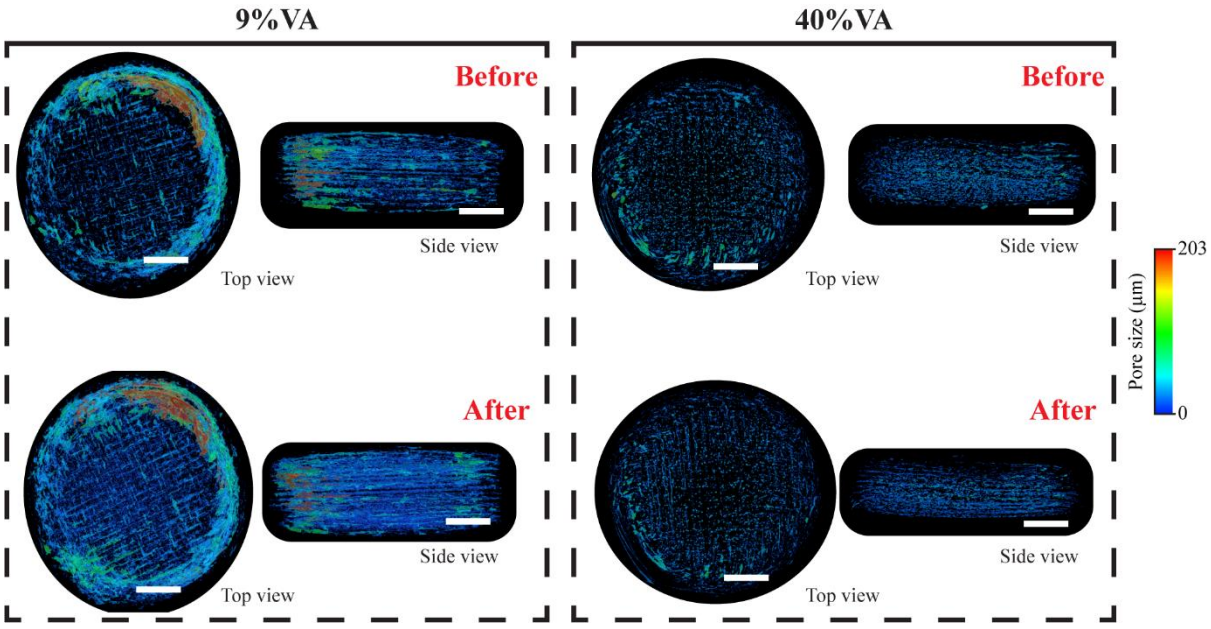

Figure 10: µCT reconstruction of the 3D printed tablets from MPT/ 9%VA and MPT/40%VA before and after dissolution with views from top and front of the tablet showing the pores. Note: white scale bar represents 2 mm.

4. Conclusion

Ethylene-vinyl acetate was successfully used for the preparation of highly drug-loaded tablets through 3D printing. DEAM technology in which pellets and powder were used as feedstock materials showed more formulation freedom compared with FFF due to the limitations of both mechanical and rheological properties. Drug-loaded filaments failed FFF due to inappropriate mechanical properties when the filament was not sufficiently stiff to act as a piston for continuous feeding. In addition, the high melt viscosity for some drug-loaded filaments was a drawback for the constant flow. These properties were highly dependent on the EVA grade.

The mechanical and rheological properties were non-limiting steps for DEAM technology as the screw rotation drives the material flow. This process enables the provision of enough pressure to overcome the high melt viscosity of the formulation. Powder-DEAM was also promising, but many challenges were encountered due to poor powder flowability and inconvenient cleaning. The move from filament-based to screw-based 3D printing seems to be the next major step for this technology as this allows the exploration of more formulations that were not processable via conventional filament-based 3D printing due to their poor mechanical properties. This will increase the potential applications that can benefit from the outstanding capabilities of 3D printing in the medical field.

Acknowledgment

The Authors acknowledge the support of Celanese™ and Dr. Christian Schneider for providing the EVA samples.

The Ghent University Special Research Fund (BOF-UGent) is acknowledged for the support of the Centre of Expertise UGCT (BOF.EXP.2017.0007) and for the financial support through project BOF.24Y.2018.0007.

References

[1] S. Bandari, D. Nyavanandi, N. Dumpa, M.A. Repka, Coupling hot melt extrusion and fused deposition modeling: Critical properties for successful performance, Adv. Drug Deliv. Rev. 172 (2021) 52–63. https://doi.org/10.1016/j.addr.2021.02.006.

[2] S. Cailleaux, N.M. Sanchez-Ballester, Y.A. Gueche, B. Bataille, I. Soulairol, Fused Deposition Modeling (FDM), the new asset for the production of tailored medicines, J. Control. Release. 330 (2021) 821–841. https://doi.org/10.1016/j.jconrel.2020.10.056.

[3] A. Melocchi, M. Uboldi, M. Cerea, A. Foppoli, A. Maroni, S. Moutaharrik, L. Palugan, L. Zema, A. Gazzaniga, A Graphical Review on the Escalation of Fused Deposition Modeling (FDM) 3D Printing in the Pharmaceutical Field, J. Pharm. Sci. 109 (2020) 2943–2957. https://doi.org/10.1016/j.xphs.2020.07.011.

[4] N. Dumpa, A. Butreddy, H. Wang, N. Komanduri, S. Bandari, M.A. Repka, 3D printing in personalized drug delivery: An overview of hot-melt extrusion-based fused deposition modeling, Int. J. Pharm. 600 (2021) 120501. https://doi.org/10.1016/j.ijpharm.2021.120501.

[5] C. Parulski, O. Jennotte, A. Lechanteur, B. Evrard, Challenges of fused deposition modeling 3D printing in pharmaceutical applications: Where are we now?, Adv. Drug Deliv. Rev. 175 (2021). https://doi.org/10.1016/j.addr.2021.05.020.

[6] J. Macedo, A. Samaro, V. Vanhoorne, C. Vervaet, J.F. Pinto, Processability of poly(vinyl alcohol) Based Filaments With Paracetamol Prepared by Hot-Melt Extrusion for Additive Manufacturing, J. Pharm. Sci. 109 (2020) 3636–3644. https://doi.org/10.1016/j.xphs.2020.09.016.

[7] A. Samaro, P. Janssens, V. Vanhoorne, J. Van Renterghem, M. Eeckhout, L. Cardon, T. De Beer, C. Vervaet, Screening of pharmaceutical polymers for extrusion-Based Additive Manufacturing of patient-tailored tablets, Int. J. Pharm. 586 (2020) 119591. https://doi.org/10.1016/j.ijpharm.2020.119591.

[8] S.J. Trenfield, A. Awad, A. Goyanes, S. Gaisford, A.W. Basit, 3D Printing Pharmaceuticals: Drug Development to Frontline Care, Trends Pharmacol. Sci. 39 (2018) 440–451. https://doi.org/10.1016/j.tips.2018.02.006.

[9] E. Fuenmayor, M. Forde, A. V. Healy, D.M. Devine, J.G. Lyons, C. McConville, I. Major, Material considerations for fused-filament fabrication of solid dosage forms, Pharmaceutics. 10 (2018) 1–27. https://doi.org/10.3390/pharmaceutics10020044.

[10] A. Melocchi, F. Briatico-Vangosa, M. Uboldi, F. Parietti, M. Turchi, D. von Zeppelin, A. Maroni, L. Zema, A. Gazzaniga, A. Zidan, Quality considerations on the pharmaceutical applications of fused deposition modeling 3D printing, Int. J. Pharm. 592 (2021) 119901. https://doi.org/10.1016/j.ijpharm.2020.119901.

[11] J. Aho, J.P. Bøtker, N. Genina, M. Edinger, L. Arnfast, J. Rantanen, Roadmap to 3D-Printed Oral Pharmaceutical Dosage Forms: Feedstock Filament Properties and Characterization for Fused Deposition Modeling, J. Pharm. Sci. 108 (2019) 26–35. https://doi.org/10.1016/j.xphs.2018.11.012.

[12] B. Shaqour, M. Abuabiah, S. Abdel-fattah, A. Juaidi, R. Abdallah, W. Abuzaina, M. Qarout, B. Verleije, P. Cos, Gaining a better understanding of the extrusion process in fused filament fabrication 3D printing : a review, Int. J. Adv. Manuf. Technol. (2021). https://doi.org/https://doi.org/10.1007/s00170-021-06918-6.

[13] G. Verstraete, A. Samaro, W. Grymonpré, V. Vanhoorne, B. Van Snick, M.N. Boone, T. Hellemans, L. Van Hoorebeke, J.P. Remon, C. Vervaet, 3D printing of high drug loaded dosage forms using thermoplastic polyurethanes, Int. J. Pharm. 536 (2018) 318–325. https://doi.org/10.1016/j.ijpharm.2017.12.002.

[14] E. Prasad, M.T. Islam, D.J. Goodwin, A.J. Megarry, G.W. Halbert, A.J. Florence, J. Robertson, Development of a hot-melt extrusion (HME) process to produce drug loaded Affinisol™ 15LV filaments for fused filament fabrication (FFF) 3D printing, Addit. Manuf. 29 (2019) 100776. https://doi.org/10.1016/j.addma.2019.06.027.

627 [15] P. Xu, J. Li, A. Meda, F. Osei-Yeboah, M.L. Peterson, M. Repka, X. Zhan, Development of a
628 quantitative method to evaluate the printability of filaments for fused deposition modeling 3D
629 printing, Int. J. Pharm. 588 (2020) 119760. https://doi.org/10.1016/j.ijpharm.2020.119760.
630 [16] S. Wang, L. Capoen, D.R. D'hooge, L. Cardon, Can the melt flow index be used to predict the
631 success of fused deposition modelling of commercial poly(lactic acid) filaments into 3D printed
632 materials?, Plast. Rubber Compos. 47 (2018) 9–16.
633 https://doi.org/10.1080/14658011.2017.1397308.
634 [17] S. Whyman, K.M. Arif, J. Potgieter, Design and development of an extrusion system for 3D
635 printing biopolymer pellets, Int. J. Adv. Manuf. Technol. 96 (2018) 3417–3428.
636 https://doi.org/10.1007/s00170-018-1843-y.
637 [18] A. La Gala, R. Fiorio, M. Erkoç, L. Cardon, D.R. D'hooge, Theoretical evaluation of the melting
638 efficiency for the single-screw micro-extrusion process: The case of 3D printing of abs,
639 Processes. 8 (2020) 1–22. https://doi.org/10.3390/pr8111522.
640 [19] A. Goyanes, N. Allahham, S.J. Trenfield, E. Stoyanov, S. Gaisford, A.W. Basit, Direct powder
641 extrusion 3D printing: Fabrication of drug products using a novel single-step process, Int. J.
642 Pharm. 567 (2019). https://doi.org/10.1016/j.ijpharm.2019.118471.
643 [20] M. Fanous, S. Gold, S. Muller, S. Hirsch, J. Ogorka, G. Imanidis, Simplification of fused deposition
644 modeling 3D-printing paradigm: Feasibility of 1-step direct powder printing for immediate
645 release dosage form production, Int. J. Pharm. 578 (2020) 119124.
646 https://doi.org/10.1016/j.ijpharm.2020.119124.
647 [21] B. Shaqour, I. Reigada, Z. Górecka, E. Choińska, B. Verleije, K. Beyers, W. Świeszkowski, A.
648 Fallarero, P. Cos, 3D-printed drug delivery systems: The effects of drug incorporation methods
649 on their release and antibacterial efficiency, Materials (Basel). 13 (2020) 1–16.
650 https://doi.org/10.3390/ma13153364.
651 [22] A. Almeida, S. Possemiers, M.N. Boone, T. De Beer, T. Quinten, L. Van Hoorebeke, J.P. Remon,
652 C. Vervaet, Ethylene vinyl acetate as matrix for oral sustained release dosage forms produced
653 via hot-melt extrusion, Eur. J. Pharm. Biopharm. 77 (2011) 297–305.
654 https://doi.org/10.1016/j.ejpb.2010.12.004.
655 [23] N. Genina, J. Holländer, H. Jukarainen, E. Mäkilä, J. Salonen, N. Sandler, Ethylene vinyl acetate
656 (EVA) as a new drug carrier for 3D printed medical drug delivery devices, Eur. J. Pharm. Sci. 90
657 (2016) 53–63. https://doi.org/10.1016/j.ejps.2015.11.005.
658 [24] J.M. Nasereddin, N. Wellner, M. Alhijjaj, P. Belton, S. Qi, Development of a Simple Mechanical
659 Screening Method for Predicting the Feedability of a Pharmaceutical FDM 3D Printing Filament,
660 Pharm. Res. 35 (2018). https://doi.org/10.1007/s11095-018-2432-3.
661 [25] G. Ćwikła, C. Grabowik, K. Kalinowski, I. Paprocka, P. Ociepka, The influence of printing
662 parameters on selected mechanical properties of FDM/FFF 3D-printed parts, IOP Conf. Ser.
663 Mater. Sci. Eng. 227 (2017). https://doi.org/10.1088/1757-899X/227/1/012033.
664 [26] L. Santana, J. Lino Alves, A. da Costa Sabino Netto, A study of parametric calibration for low
665 cost 3D printing: Seeking improvement in dimensional quality, Mater. Des. 135 (2017) 159–
666 172. https://doi.org/10.1016/j.matdes.2017.09.020.
667 [27] N. Mobaraki, J.M. Amigo, HYPER-Tools. A graphical user-friendly interface for hyperspectral
668 image analysis, Chemom. Intell. Lab. Syst. 172 (2018) 174–187.
669 https://doi.org/10.1016/j.chemolab.2017.11.003.
670 [28] M. Vidal, J.M. Amigo, Pre-processing of hyperspectral images. Essential steps before image
671 analysis, Chemom. Intell. Lab. Syst. 117 (2012) 138–148.
672 https://doi.org/10.1016/j.chemolab.2012.05.009.
673 [29] Y. Roggo, A. Edmond, P. Chalus, M. Ulmschneider, Infrared hyperspectral imaging for
674 qualitative analysis of pharmaceutical solid forms, Anal. Chim. Acta. 535 (2005) 79–87.
675 https://doi.org/10.1016/j.aca.2004.12.037.
676 [30] B. Masschaele, M. Dierick, D. Van Loo, M.N. Boone, L. Brabant, E. Pauwels, V. Cnudde, L. Van
677 Hoorebeke, HECTOR: A 240kV micro-CT setup optimized for research, J. Phys. Conf. Ser. 463

(2013). https://doi.org/10.1088/1742-6596/463/1/012012.
[31] J. Vlassenbroeck, M. Dierick, B. Masschaele, V. Cnudde, L. Van Hoorebeke, P. Jacobs, Software tools for quantification of X-ray microtomography at the UGCT, Nucl. Instruments Methods Phys. Res. Sect. A Accel. Spectrometers, Detect. Assoc. Equip. 580 (2007) 442–445. https://doi.org/10.1016/j.nima.2007.05.073.
[32] L. Wang, P. Fang, C. Ye, J. Feng, Solid-State NMR Characterizations on Phase Structures and Molecular Dynamics of Poly(ethylene-co-vinyl acetate), J. Polym. Sci. Part B Polym. Phys. 44 (2006) 2864–2879. https://doi.org/10.1002/polb.
[33] J. Zhang, P. Xu, A.Q. Vo, S. Bandari, F. Yang, T. Durig, M.A. Repka, Development and evaluation of pharmaceutical 3D printability for hot melt extruded cellulose-based filaments, J. Drug Deliv. Sci. Technol. 52 (2019) 292–302. https://doi.org/10.1016/j.jddst.2019.04.043.
[34] S. Henry, A. Samaro, F.H. Marchesini, B. Shaqour, J. Macedo, V. Vanhoorne, C. Vervaet, Extrusion-based 3D printing of oral solid dosage forms: material requirements and equipment dependencies, Int. J. Pharm. 598 (2021) 120361. https://doi.org/10.1016/j.ijpharm.2021.120361.
[35] M.P. Serdeczny, R. Comminal, D.B. Pedersen, J. Spangenberg, Experimental and analytical study of the polymer melt flow through the hot-end in material extrusion additive manufacturing, Addit. Manuf. 32 (2020) 100997. https://doi.org/10.1016/j.addma.2019.100997.
[36] B. Shaqour, A. Samaro, B. Verleije, K. Beyers, C. Vervaet, P. Cos, Production of drug delivery systems using fused filament fabrication: A systematic review, Pharmaceutics. 12 (2020) 1–16. https://doi.org/10.3390/pharmaceutics12060517.
[37] G. Hodgson, A. Ranellucci, J. Moe, Slic3r Manual, (2011). https://manual.slic3r.org/expert-mode/filament-settings.
[38] M. Saviano, R.P. Aquino, P. Del Gaudio, F. Sansone, P. Russo, Poly(vinyl alcohol) 3D printed tablets: The effect of polymer particle size on drug loading and process efficiency, Int. J. Pharm. 561 (2019) 1–8. https://doi.org/10.1016/j.ijpharm.2019.02.025.
[39] M.I. Calafel, R.H. Aguirresarobe, N. Sadaba, M. Boix, J.I. Conde, B. Pascual, A. Santamaria, Tuning the viscoelastic features required for 3D printing of PVC-acrylate copolymers obtained by single electron transfer-degenerative chain transfer living radical polymerization (SET-DTLRP), Express Polym. Lett. 12 (2018) 824–835. https://doi.org/10.3144/expresspolymlett.2018.70.
[40] I. Calafel, R.H. Aguirresarobe, M.I. Peñas, A. Santamaria, M. Tierno, J.I. Conde, B. Pascual, Searching for Rheological Conditions for FFF 3D Printing with PVC Based Flexible Compounds, Materials (Basel). 13 (2020) 178. https://doi.org/10.3390/ma13010178.

Supplementary data

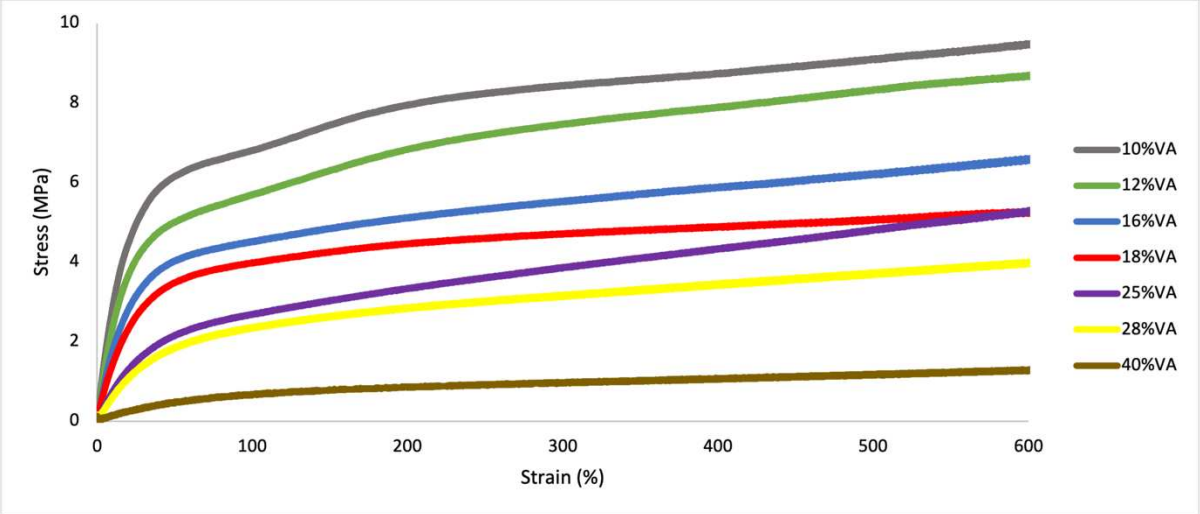

Figure S 1: Stress-strain curves for pure EVA filaments obtained from tensile test

Formulation	Picture
Filament	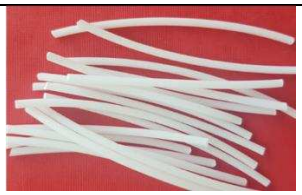
Pellets	
FFF 3D printed tablet	

Pellets-DEAM 3D printed tablet	
Powder-DEAM 3D printed tablet	

724 *Table S 1: Pictures for different MPT/EVA (50/50;* w/w*%) using 18%VA.*